Vol. 47, No. 4 (2025) 753-767, DOI: 10.24874/ti.2021.09.25.11

Tribology in Industry

www.tribology.rs

RESEARCH

Effect of Waviness Contact on Sliding Friction of the Piston-Cylinder System in Mixed Lubrication

Mohamed Benbrik[a], Mohamed Bouzit[b], Miloud Tahar Abbès[a, *], Patrick Maspeyrot[c]

[a]*Laboratory of Mechanical and Energy, Faculty of Technology, University Hassiba Benbouali of Chlef, Algeria,*
[b]*Faculty of Mechanical Engineering, USTOran, Algeria,*
[c]*Department of Mechanics and complex systems, Faculty of Sciences, University of Poitiers, Futuroscope, France.*

Keywords:

Mixed lubrication
Waviness contact
Sliding contact friction
Skirt cylinder experiment friction
Frictional energy loss

* Corresponding author:

Miloud Tahar Abbès
E-mail : taharabbes@yahoo.fr

Received: 11 September 2025
Revised: 20 October 2025
Accepted: 19 November 2025

A B S T R A C T

The piston-cylinder is the main component of the transmission of energy in the vehicle's engine, but it represents a significant source of unavoidable friction, which negatively affects engine performance by reducing piston lifespan and increasing fuel consumption. To determine the effect of lubrication performance and asperity contact on the tribological characteristics, mainly on the friction generated by asperity sliding contact, a numerical model of a real piston cylinder operating in mixed lubrication was developed. The mixed lubrication analysis shows the necessity to take into account the elasticity of the piston skirt-cylinder as well as for cavitation to ensure the consistency of the results. The sliding friction, resulting from the Johnson contact model, is developed, with a new approach, according to the Bowden-Tabor friction model. An experimental method is employed to determine the coefficient of the sliding friction. The results show that the tribological characteristics—contact pressure, sliding contact friction, energy loss, and the coefficient of sliding contact friction—are influenced by the waviness of the contact surface. When the amplitude of the asperities increases from 12 to 16 µm, the coefficient of the sliding friction and the corresponding contact energy loss increase from 0.128 to 0.16 and from 0.054 J to 1.126 J, respectively, representing 25% to 78% of the total energy loss.

1. INTRODUCTION

Friction in the piston-cylinder system plays an important role in engine efficiency and constitutes 20-40% of the total friction in the engine [1-3]. Friction is related to energy loss and therefore to fuel consumption, with about 33% of the fuel energy being used to overcome friction in the engine, and about 45% of this energy occurs in the piston unit, including the piston skirt [4,5]. The lost fuel consumption, in addition to having a significant impact on economic reliability, contributes even more through two types of emissions: harmful gases that increase air pollution and thus affect human health [6] and greenhouse gases that cause global warming, leading to negative impacts on the earth's climate [7,8]. It is therefore necessary to develop a realistic model of piston behavior under the most severe operating condition—mixed lubrication—in order to better understand and then to provide appropriate solutions for reducing friction at the piston-cylinder interface. The problem has been the subject of several studies and continues to be an active area of research today.

Early works on the skirt lubrication in mixed lubrication, considering rough surface [9,10], began in the 1980s with the works of Zhu et al. [11,12], which constitute a basic reference. The developed model is based on the average Reynolds equation presented by Patir and Cheng [13] for the mixed lubrication and Li et al. [14] for the dynamic equations. The contact friction force is calculated using the asperity contact model derived by Johnson [15]. However, in this basic study, cavitation, which has an important effect on the results, was not taken into account.

It was not until around 2012 that a few models on mixed lubrication for analyzing piston skirt cylinder contact were developed. Jin et al. [16] presented a numerical analysis of piston slap modeled as a lateral contact by a function implemented in ABAQUS software, in which a condition limiting the maximum slap is included in the contact slap. Ning et al. [17] conducting a theoretical analysis of piston skirts in mixed lubrication, examining the shear-thinning effect of multigrade lubricants on the friction. Sun et al. [18] analyzed lubrication performance by comparing the piston skirt–cylinder liner frictional pair in flooded status with the actual lubricant transport occurring during the piston's upstroke. The friction pair is performed by the viscous friction force of the oil film and the contact friction force of the rough surfaces, according to the asperity contact model developed by Greenwood and Trip [19]. Meng et al. [20] developed a mixed-lubrication model for the piston skirt by considering the break-in period and its effect on the tribological characteristics. The contact model uses the wave asperities with a trapezoidal shape resulting from wear of the original triangle shape. The corresponding averaged Reynolds equation is expressed using a new set of the lubricant flow factors for both the original and the worn waviness asperity. More recently, Liu et al. [21] established a dynamic friction model in which they analyzed the effect of ring and cylinder liner on average friction using experimental Box-Behnken response surface methodology. In the above studies, the authors considered only the effect of the skirt profile without accounting for piston and cylinder deformation or cavitation. To analyze cylinder liner vibration using Multibody Dynamics Physical Field applied to the crank, connecting rod, and piston–cylinder system, Zhao et al. [22] incorporated mixed lubrication, introducing asperity-contact friction as external forces in the multibody dynamic equations. In calculating the contact friction force, the authors state that the friction coefficient is determined experimentally, but they provide no information regarding how it was obtained.

Addressing the behavior of the piston–cylinder system with respect to the issues discussed above depends mainly on how to understand and develop a realistic model of the piston-cylinder behavior. The aim is to evaluate the effect of surface waviness on the tribological characteristics, mainly sliding contact friction, in order to improve piston–cylinder design. To achieve this objective, the following approaches are adopted in the present work. A numerical method is developed to determine how the piston begins to operate in the mixed lubrication regime for a given waviness asperity and engine speed. The sliding contact friction, resulting from the Johnson contact model, is formulated according to Bowden-Tabor friction theory [23] for a given asperity amplitude. An experimental method is used to determine the coefficient of sliding friction of the piston-cylinder for a given surface of a known waviness amplitude.

An application is carried out on a real case of a piston-cylinder system of a V8 air-cooled diesel engine type F8L413 mounted on the TB 230 heavy truck of the DVP Company in Algeria.

2. FORMULATION

2.1 Basic governing equations

The movement of the piston in the cylinder consists of a main axial movement, with amplitude equal to half the crankshaft stroke, that produces the engine's work output, and a secondary movement with an amplitude on the order of the piston-cylinder clearance, caused by the imbalance of forces and moments about the wrist-pin off-set. The secondary movement is described by the top and bottom skirt eccentricity, respectively $e_t(t)$ and $e_b(t)$, with amplitudes less than the radial clearance, resulting from the lateral displacement of the piston and its rotation around the wrist-pin offset. The different interactions of the piston-cylinder in mixed lubrication are represented in the model shown in Figure 1a.

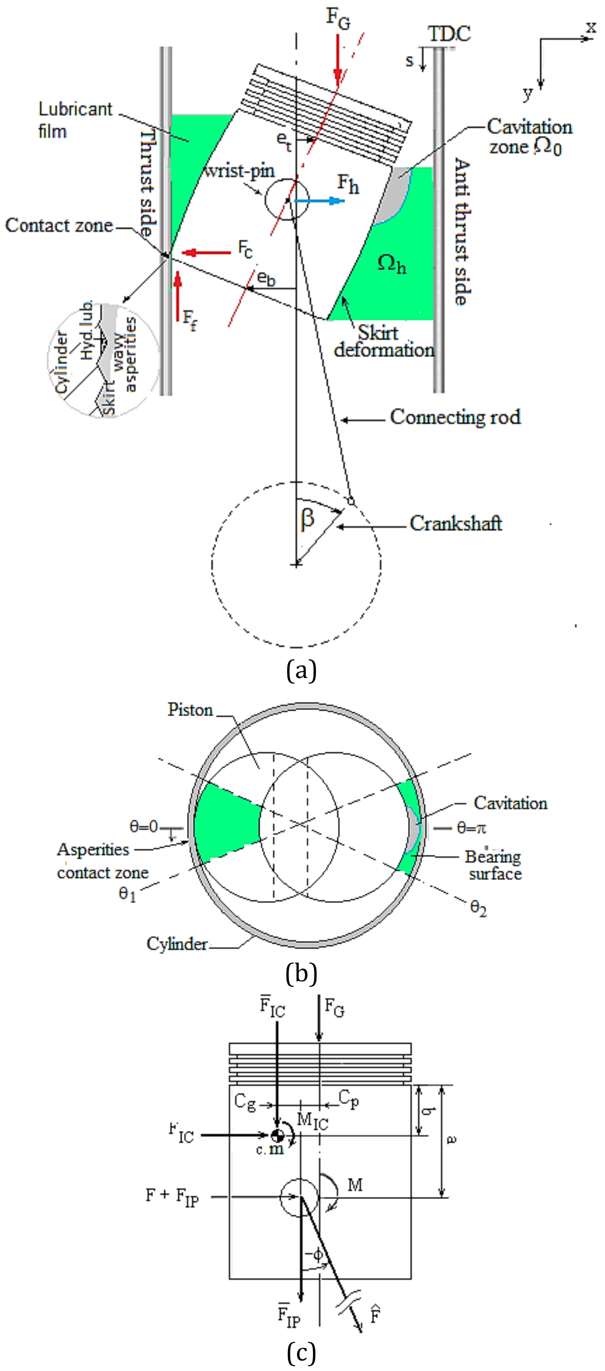

Fig. 1. Schematic representation of the piston-cylinder in mixed lubrication (a) schematic diagram of the piston-cylinder block movement, (b) lubrication domain Ω_h in circumferential direction, (c) force analysis diagram.

The piston model is formulated using the following three equations: two dynamic equations for the piston eccentricities $e_t(t)$ and $e_b(t)$, and the universal average Reynolds equation for pressure $p_h\,(x,y)$ in mixed lubrication [11-13,24], including the effect of cavitation [25].

$$\begin{aligned}\left[m_{pist}\left(1-\frac{b}{L}\right)+m_{pin}\left(1-\frac{a}{L}\right)\right]\ddot{e}_t \\ +\left[m_{pist}\frac{b}{L}+m_{pin}\frac{a}{L}\right]\ddot{e}_b \\ =F_h+F_c \\ +\left(F_G+\bar{F}_{IP}+\bar{F}_{IC}+F_f\right)tan\phi\end{aligned} \tag{1}$$

$$\begin{aligned}\left[\frac{I_{pist}}{L}+m_{pist}(a-b)\left(1-\frac{b}{L}\right)\right]\ddot{e}_t \\ -\left[\frac{I_{pist}}{L}+m_{pist}(a-b)\left(\frac{b}{L}\right)\right]\ddot{e}_b \\ =M_h+M_c+F_GC_P-\bar{F}_{IC}C_g \\ +M_f\end{aligned} \tag{2}$$

$$\begin{aligned}\left[\frac{I_{pist}}{L}+m_{pist}(a-b)\left(1-\frac{b}{L}\right)\right]\ddot{e}_t \\ -\left[\frac{I_{pist}}{L}+m_{pist}(a-b)\left(\frac{b}{L}\right)\right]\ddot{e}_b \\ =M_h+M_c+F_GC_P-\bar{F}_{IC}C_g \\ +M_f\end{aligned} \tag{3a}$$

Where F is a switch function and D is the universal variable accounting for the cavitation, defined as:

$$D=p_h \qquad \text{F=1 in the active zone} \tag{3b}$$

$$D=h^*-h,\quad h^*=h\frac{\rho_c}{\rho_f} \qquad \text{F=0 in the cavitation zone} \tag{3c}$$

h^* is the filling ratio or the equivalent film thickness.

The boundary conditions for the universal average Reynolds equation are, respectively, the pressure symmetry condition, the pressure boundary condition in the circumferential direction, the pressure boundary conditions at the upper and the lower ends of the piston skirt, and the pressure boundary cavitation.

$$\begin{gathered}\left.\frac{\partial p_h}{\partial}\right|_{\theta=0}=\left.\frac{\partial p_h}{\partial y}\right|_{\theta=\pi}=0 \\ p_h=0\;\theta_1<\theta<\theta_2 \\ p_h(\theta,0)=p_h(\theta,L)=0 \\ p=p_{cav},\quad \left.\frac{\partial p}{\partial n}\right|_{(x,y)=(x_r,y_r)}\end{gathered} \tag{3d}$$

The full film thickness h is defined by:

$$\begin{aligned} \mathrm{h}\,(\theta, \mathrm{y}, \mathrm{t}) = c + e_t(t)cos\theta & \\ + \frac{y}{L}[e_t(\mathrm{t}) - e_b(\mathrm{t})]cos\theta + f(y) & \\ + \mathrm{d}(\theta, \mathrm{y}, \mathrm{t}) + \mathrm{d_s}(\theta, \mathrm{y}, \mathrm{t}) & \end{aligned} \tag{4}$$

where the terms $\mathrm{d_c}(\theta, \mathrm{y}, \mathrm{t})$ and $\mathrm{d_s}(\theta, \mathrm{y}, \mathrm{t})$ represent the elastic deformations of the cylinder and the piston skirt, respectively, due to the contact and hydrodynamic pressures. Using the force method in structural mechanics, the elastic deformations are expressed by:

$$\mathrm{d_c}(\theta, \mathrm{y}, \mathrm{t}) = \iint_{\Omega_c} \mathrm{C_c}\,(\theta, \mathrm{y}, \xi, \eta)\mathrm{p_c}\,(\xi, \eta, \mathrm{t})\mathrm{d}\xi\mathrm{d}\eta \tag{5a}$$

$$\mathrm{d_s}(\theta, \mathrm{y}, \mathrm{t}) = \iint_{\Omega_h} \mathrm{C_s}\,(\theta, \mathrm{y}, \xi, \eta)\,\mathrm{p_h}\,(\xi, \eta, \mathrm{t})\mathrm{d}\xi\mathrm{d}\eta \tag{5b}$$

The coefficients φ_x, φ_y and φ_s are the flow factors used to take into account the influence of the surface waviness on partial hydrodynamic lubrication [13].

The piston-cylinder surfaces, in their finished state, are not perfectly smooth but exhibit inevitable geometric shape defects, mainly the second-order macroscopic waviness caused by machine and tool vibrations and the third-order microscopic roughness resulting from the movement of the cutting tools. The contact of the skirt asperities with the cylinder bore is modeled according to the Johnson contact model [15], which is based on the Hertz theory [26] of the elastic contact. The model describes a two-dimensional blunt wedge (the skirt) indenting an elastic half-space plane (the cylinder).

In this work, only the waviness profile is taken into account. The indentation effect of the roughness, whose amplitude is at least one order of magnitude smaller than that of the waviness, is neglected relative to the indentation effect of the waviness [11]. Furthermore, the waviness profile must have a smooth and continuous surface in order to satisfy the linear elasticity assumptions of the Johnson contact model.

In the case of waviness only, the expressions of the flow factors are given in [11,27] by:

$$\varphi_x = 1 + \left(\frac{\Omega}{h}\right)^2, \varphi_y = \left[1 - \left(\frac{\Omega}{h}\right)^2\right]^2, \varphi_s = \frac{\Omega}{h} \tag{6}$$

The function $f(y)$ represents the axial profile of the piston skirt, which is barrel-shaped and described by a fourth-degree polynomial. The adopted profile shape generates a convergent–divergent gap, thereby preventing excessive pressure in the lubricant film.

2.2 The sliding friction of the contact asperities according to Bowden-Tabor model

The sliding friction force due to contact asperities has been modeled in previous works using a Coulomb solid-to-solid friction model [11,16-22]. Figure 2 shows the Johnson contact model of the skirt asperity (2) indenting the cylinder surface (1) with a given wavy contact normal deformation δ. The skirt surface is deformed normally under the action of the normal load $\mathrm{F_c}$. When the piston moves axially, the cylinder surface is deformed by ploughing with a transverse section $\mathrm{A_t}$, by the skirt asperity, and this occurs as long as a normal deformation exists under the action of the wavy contact load $\mathrm{F_c}$.

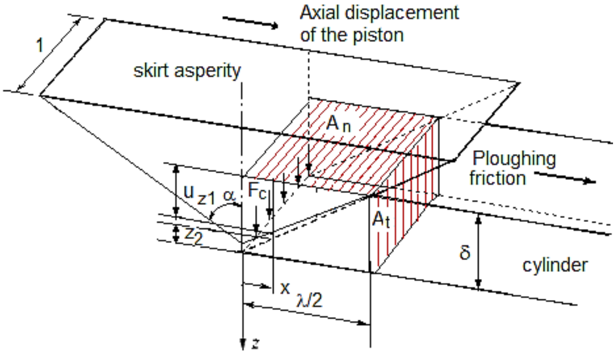

Fig. 2. Sliding friction of the wavy asperity contact.

The sliding friction force $\mathrm{F_{fc}}$ is considered as the deformation force needed to plough the cylinder surface according to the Bowden-Tabor friction model. The friction force is obtained by the relation

$$F_{fc} = \mu_P F_c \tag{7}$$

where μ_P is the coefficient of ploughing friction, defined as the ratio between the straight transverse section $\mathrm{A_t}$ and the normal section $\mathrm{A_n}$, given by:

$$\mu_P = \frac{A_t}{A_n} = \frac{2\delta}{\lambda} \tag{8}$$

The wavy contact normal load $\mathrm{F_c}$ due to solid-to-solid contact between the skirt asperities and the cylinder bore is expressed by:

$$F_c = \iint_{\Omega_c} P_c R cos\theta\, d\theta dy \tag{9}$$

where Ω_c is the wavy contact zone of the piston skirt-cylinder.

By using the model of the wavy contact asperity developed by Johnson [15], the wavy contact pressure P_c is the solution of the nonlinear equation for a given value of the wavy contact deformation δ during contact deformation [11]

$$\frac{P_c}{\bar{E}}\left[-k_1 \ln\left(\frac{F_c}{\bar{E}}\frac{\lambda}{4\Omega}\right)+k_2\right]-\delta=0 \qquad (10)$$

where $k_1 = 0.635$ and $k_2 = 1.0556$ are constants of numerical integration of the wavy contact variable δ [11,15].

As shown in Figure 2, the wavy contact deformation δ represents the sum of the normal displacement $u_{z1}(x)$ due to the distributive normal pressure p(x) over the interval $(-\lambda/2 \leq x \leq \lambda/2)$ in the straight transverse section of the cylinder, the skirt deformation of the asperity $u_{z2}(x)$ and the wedge profile $z_2(x)$ of the asperity.

Related to the mean thickness $\bar{h}$ and the profile $z_2(x)$, the wavy deformation is expressed by [28]:

$$\delta = z_2(x) - \bar{h}\,(x,y), \Omega > \bar{h} \qquad (11)$$

The total sliding contact friction force F_{fc} of all contact asperities in the domain Ω_c of the skirt when the piston moves with an axial speed U, is given at crank angle step by:

$$F_{fc} = -\frac{|U|}{U}\mu_p \iint_{\Omega_c} P_c R\, d\theta dy \qquad (12)$$

When taking into account the cavitation, the hydrodynamic friction load F_{fh} at a crank angle step is given by:

$$F_{fh} = \iint_{\Omega_h} \tau_h \frac{h^*}{h} R\, d\theta dy \qquad (13)$$

h^* is the filling ratio and τ_h is the shear stress in the lubricant fluid film, given by:

$$\tau_h = -\frac{\mu_h U}{h}\left(\phi_h + \phi_{fs}\right) + \frac{h}{2}\phi_p \frac{\partial p_h}{\partial y} \qquad (14)$$

The total skirt friction force is the sum of the sliding contact friction F_{fc} and the hydrodynamic friction force F_{fh}.

The coefficients ϕ_h, ϕ_{fs} and ϕ_p represent the flow shear stress factors for roughness and waviness surfaces effects. The calculation of the coefficients for only the waviness effect is given in references [11] and [27].

2.3 Lost contact energy

The total energy loss by friction E_f produced in one engine cycle is the sum of the lost contact energy E_c due to contact friction and the lost hydrodynamic energy E_h due to hydrodynamic friction:

$$E_f = \int_{cycle} \left(\left|F_{fh}\right| + \left|F_{fc}\right|\right) ds \qquad (15)$$

where s is the axial displacement of the piston. The variable s is related to the crankshaft rotation β by the following relationship:

$$s(\beta) = r + L - r\cos\beta - L\left(1 - \frac{r^2}{L^2}\sin^2\beta\right)^{0.5} \qquad (16)$$

When solving the piston lubrication problem, the crank angle β of the crankshaft is discretized in a finite crank angle step $\Delta\beta$. Using equation (16), the axial displacement of the piston at each crank angle step $\Delta\beta$ is expressed by:

$$s(\Delta\beta) = r + L - r cos(\Delta\beta) - L\left(1 - \frac{r^2}{L^2} sin^2(\Delta\beta)\right)^{0.5} \qquad (17)$$

2.4 Contact and hydrodynamic load

The contact thrust load is given by equation (9), and the hydrodynamic thrust load is given by

$$F_h = \iint_{\Omega_h} p_h R cos\theta\, d\theta dy \qquad (18)$$

Where p_h is the average hydrodynamic pressure given by the solution of the universal average Reynolds equation (3a).

3. SOLVING METHOD

The solution method is an iterative procedure in both time and space to solve the set of equations (1-3) over one engine cycle.

For a fixed cycle, at each time step, the actual solution $(e_t(t), e_b(t))$ is related to the solution at the two previous steps by using a backward finite difference scheme for the acceleration terms $\ddot{e}_t(t)$ and $\ddot{e}_b(t)$. The cavitation is solved iteratively at each step crank angle by using the modified Murty algorithm [29,30]. The algorithm ensures the conservation of flow rate across the boundaries of the cavitation region. It is simple to implement and requires little computation time compared to other methods, the most important of which is Elrod's method [31]. Three iterations are required at each time step to ensure that the cavitation region remains unchanged [25]. The cavitation zone is evaluated by computing the filling ratio $h^*(i, j)$ at the points (i, j) of the finite difference grid of the lubricant film. At each iteration step of the cavitation loop, the nonlinear set of equations (1-3) is solved numerically using the Newton-Raphson method. The solution needs 3 to 4 iterations to converge, with a residual vector satisfying $\{R\}<10^{-8}$. Thus, the full film thickness h is calculated using relation (4), where the deformations d_c and d_s are computed by equations (5a)-(5b) using the compliance matrix for the piston and the cylinder.

Once the thickness film h(t) is obtained and the contact condition $\Omega > h(t))$ is satisfied, the contact pressure $P_c(h(t))$ is calculated according to the wavelength λ and the amplitude Ω of the asperity by solving the nonlinear equation (10) using the Newton-Raphson method. In equation (10), for each film thickness, the equivalent contact condition for $\Omega > h(t)$ is introduced as $\bar{\delta} = \frac{\Omega - h}{\Omega}$.

The friction forces are determined by numerical integration of the Eq. (12)-(13). The maximum value of μ_{Pmax} is obtained by substituting in equation (11) the wavy contact deformation δ with its maximum value $\delta_{max} = 2\Omega$, together with $z_{2max} \leq 2\Omega$ and $\bar{h}_{min}(x, y) = 0$. Accordingly, the coefficient of ploughing friction given by equation (8) is bounded by its maximum value $\mu_{Pmax} \leq \frac{4\Omega}{\lambda}$.

The total energy loss by contact and hydrodynamic friction is given by equation (15) and calculated numerically at the final converged engine cycle.

A computer program implementing the adopted procedure is applied to a real piston-cylinder system of a V8 air-cooled diesel engine used in heavy trucks.

3.1 Friction experimental method

The coefficient of sliding friction of a solid-to-solid contact is measured using a variable incidence tribometer [32-33]. The device shown in Figure 3 is designed to approximately reproduce the sliding friction model between the skirt asperity and the cylinder.

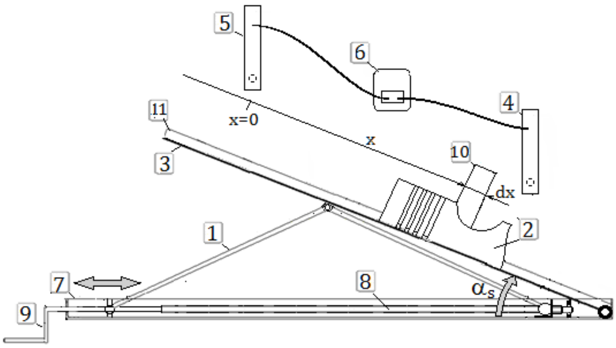

(a)

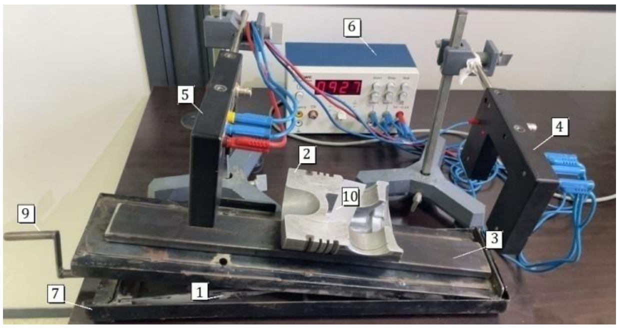

(b)

Fig. 3. Measurement of the coefficient of sliding friction in a piston-cylinder system using a variable-incidence tribometer, (a) simplified diagram of the measurement device (b) practical realization of the measurement device.

The inclined plane (11), on which a rectangular plate (3), representing the cylinder, is lifted at a low uniform velocity using the worm screw (8) and triangle (1) mechanism. Based on Coulomb's law, the measurement device allows the static and dynamic coefficients of friction to be determined by gradually increasing the angle of the inclined plane (3) until the piston (2) begins to move downwards with sliding friction. At the strict equilibrium position, the angle of the inclined plane reaches its maximum value α_s, from which the static coefficient of friction is determined by:

$$\mu_s = \tan\alpha_s \tag{19}$$

When the piston starts moving downwards, the coefficient of sliding friction μ_d can be calculated by the following relation:

$$\mu_d = \mu_s - \frac{v(t)^2 - v_0^2}{2x\, g\cos(\alpha_s)} \tag{20}$$

where $v(t)$ and v_0 are the instantaneous and initial piston velocities, respectively. Instantaneous speed $v(t) = \frac{dx}{dt}$ is obtained using the device of Figure 3b, which employs an horizontal light-slit sensor (4). The time interval dt is measured with a digital stopwatch (6), while dx is the differential length of the spot control screen (10).

4. RESULTS

The combustion gas pressure $P_G(t)$ acting on the piston head during one engine cycle is plotted in Fig. 4 as a function of the crank angle. The curve is obtained using specific thermodynamics and kinematic data of the actual F8L413 [25] diesel engine. The combustion gas load is calculated at each crank angle step using the relation $F_G(t) = \pi R^2 P_G(t)$ and then substituted in equations (1)-(2).

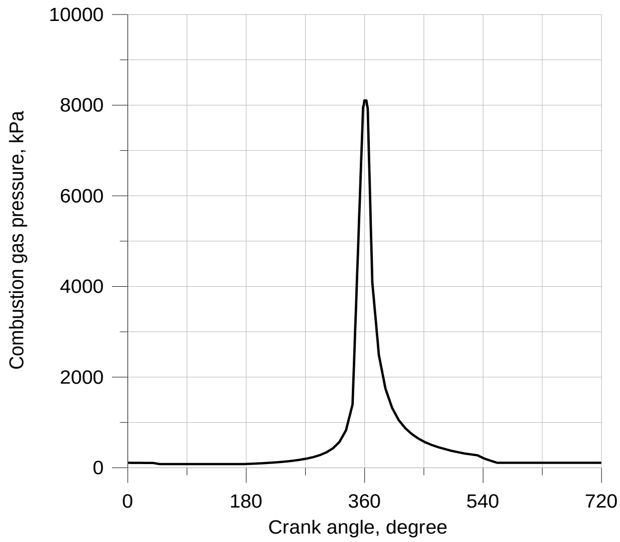

Fig. 4. Combustion gas pressure $P_G(t)$ versus crank angle β.

4.1 Contact simulation

When simulating the piston-cylinder contact, it is necessary to determine the minimum amplitude of the asperity at which contact occurs and at which the piston begins to operate in the mixed lubrication regime. To obtain this result, hydrodynamic lubrication is simulated without considering asperity contact, i.e., with $\Omega = 0$, for successive engine speeds as shown in Fig. 5. The simulation is stopped when the minimum film thickness exceeds the physical value $\Omega_{\max} =$ 10 µm, which represents the waviness amplitude of the finished surface after the break-in process [20]. The corresponding minimum values h_{min} of the minimum film thickness curves for each engine speed are listed in Table 1.

The results show that the minimum thickness satisfying the condition $h < 10$ µm is obtained for the engine speed, V=1000 rpm, where $h_{\min} =$ 9.736 µm. Thus, for engine speeds below 1000 rpm, the piston can operate in the mixed lubrication regime when the surface waviness amplitude is greater than the corresponding minimum film thickness obtained without considering asperity contact. Thus, the presented method allows us to ensure the contact according to the amplitude of the asperities and the engine speed.

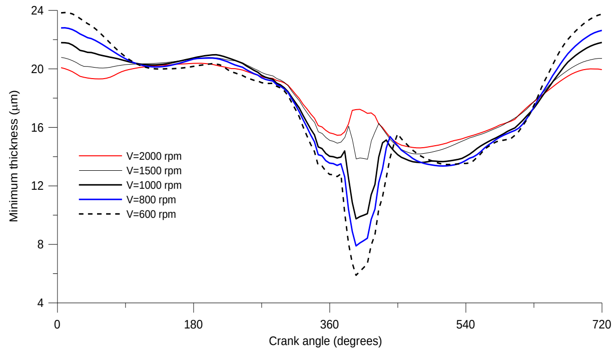

Fig. 5. Variation of the minimum film thickness for different engine speeds, considering the case without piston-cylinder contact.

Table 1. Conditions of asperity contact for different engine speeds.

V (rpm)	h_{min} (μm)	β (°)	Asperity contact
2000	14.587	480	No possible physical contact
1500	13.843	395	
1000	9.736	395	Contact for $\Omega > 9.736\ \mu m$
800	7.887	395	Contact for $\Omega > 7.887 \mu m$
600	5.877	395	Contact for $\Omega > 5.877\ \mu m$

Figure 6 shows the minimum film thickness for the cases with contact and without asperity contact for an engine speed of V=1000 rpm. An amplitude value of $\Omega = 12$µm is chosen to simulate the contact.

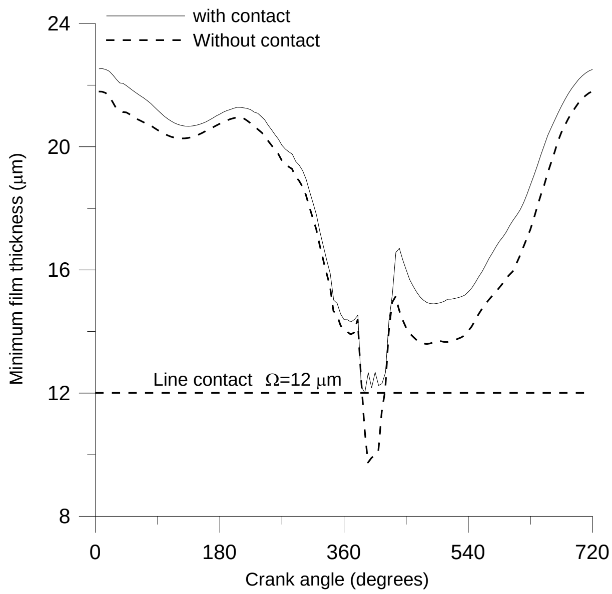

Fig. 6. Comparison of the film thickness with and without contact for an asperity amplitude of $\Omega =$ 12 µm and engine speed of V=1000 rpm.

The results show that, when contact is considered, the minimum film thickness keeps a constant value of 12 μm over a short crank angle range [385°, 420°]. This interval corresponds to the region obtained from the intersection between the contact line and the film-thickness curve without contact, as shown in Figure 6. This result demonstrates the consistency—and therefore the validity—of the method used.

4.2 Effect of the skirt elasticity and the cavitation on waviness contact

In the asperity contact model described in section 2.2, the asperities of the piston skirt surface are assumed to be rigid and to elastically deform the cylinder, which is considered elastic according to the elastic half-space contact model. The problem is whether the piston skirt should be considered elastic or rigid in order to determine the effect of skirt elasticity on asperity contact.

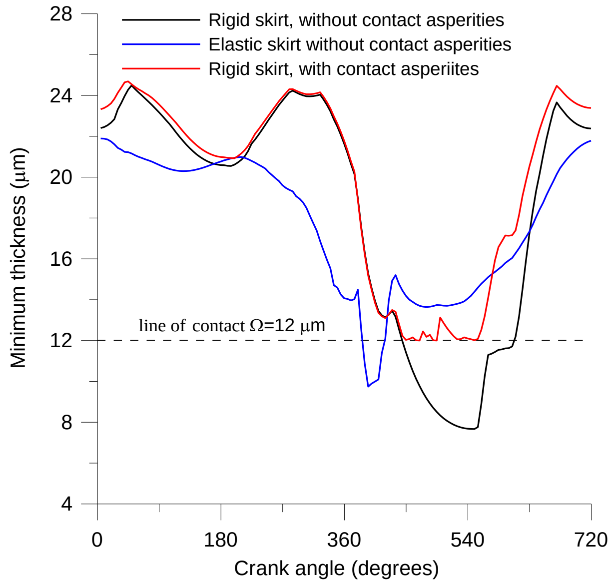

Fig. 7. Effect of skirt elasticity on the minimum film thickness with and without asperity contact for $\Omega = 12\ \mu m$.

Figure 7 shows the effect of skirt elasticity on the minimum film thickness when asperity contact is taken into account, for an engine speed of V=1000 rpm. The minimum film thickness, in the case of an elastic skirt, is 9.736 μm and occurs ATDC at a crank angle of 395°, over the short crank angle range [385°, 420°]. In the case of the rigid skirt, the lowest value of the minimum film thickness is 7.65 μm and occurs at the end of the power stroke at 550° CA over a large crank angle range [445°, 560°]. The result obtained when considering skirt elasticity is consistent with several studies [16,17,20–22], whereas the result for a rigid skirt deviates from the established findings in the piston literature. This shows the importance of taking the skirt elasticity into account to avoid results that do not correspond to the real behavior of the piston in mixed lubrication.

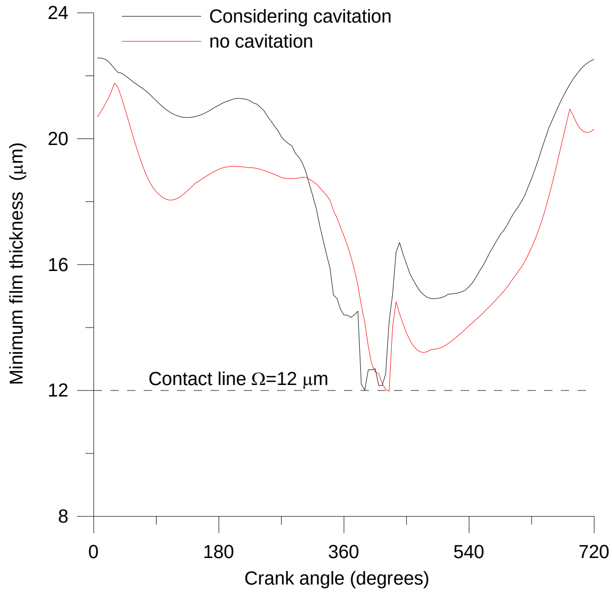

Fig. 8. Effect of the cavitation on the minimum film thickness with contact asperities and elastic skirt for amplitude $\Omega = 12\ \mu m$.

Figure 8 shows the effect of cavitation on the minimum film thickness, considering asperity contact with an amplitude of Ω=12 μm. The results show that the contact crank angle range [395°, 405°] in the case of both cavitation and asperity contact corresponds to that of the minimum film thickness, whereas when cavitation is not considered, the interval is very reduced [420°, 425°] and is not in concordance with the minimum film thickness region in the case of asperity contact. This result shows the necessity of accounting for cavitation to ensure the consistency of the results. The effect of cavitation becomes even more pronounced when the skirt is considered rigid, as the difference between the two minimum film thicknesses-for cavitation and without cavitation when asperity contact is considered-increases significantly, as shown in figure 9.

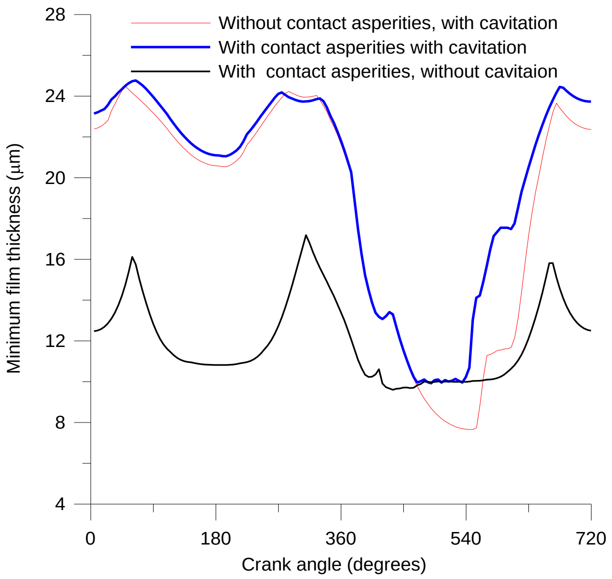

Fig. 9. Effect of cavitation on the minimum film thickness considering rigid skirt, with and without asperity contact for $\Omega = 12\ \mu m$

4.3 Effect of the waviness contact on the tribological characteristics

To study the effect of the waviness surface of the skirt on the tribological characteristics (minimum film thickness, maximum pressure, and friction), three waviness amplitudes are chosen: $\Omega_1 = 12$ μm, $\Omega_2 = 14$ μm, and $\Omega_3 = 16$ μm. The amplitudes were obtained using the contact simulation method described in section 4.1. In a first step, the amplitude is determined using Table 1 to identify the minimum value at which contact occurs for a fixed engine speed, and in a second step by incrementing the amplitudes by ΔΩ=2μm. The value of ΔΩ is chosen to ensure that the variation of the film thickness without contact gives a significant difference between the successive crank angle contact ranges.

The results presented in Figure 10 show that the minimum film thickness increases with increasing asperity amplitude. The results indicate also that the crank angle contact range becomes wider as the amplitude increases from Ω_1 to Ω_3 occurring respectively within the ranges [385°, 420°], [350°, 420°], and [340°, 430°].

Figure 11 displays the maximum contact pressure and the maximum hydrodynamic pressure for the different amplitudes Ω_1, Ω_2 and Ω_3. The maximum contact pressure and the maximum hydrodynamic pressure are obtained at each crank angle step from the distributed contact pressure $P_c\ (x, y)$ and the hydrodynamic pressure $p_h(x, y)$ at each grid point of the lubrication domain Ω_h. The maximum values are highlighted in the different curves of Figure 11.

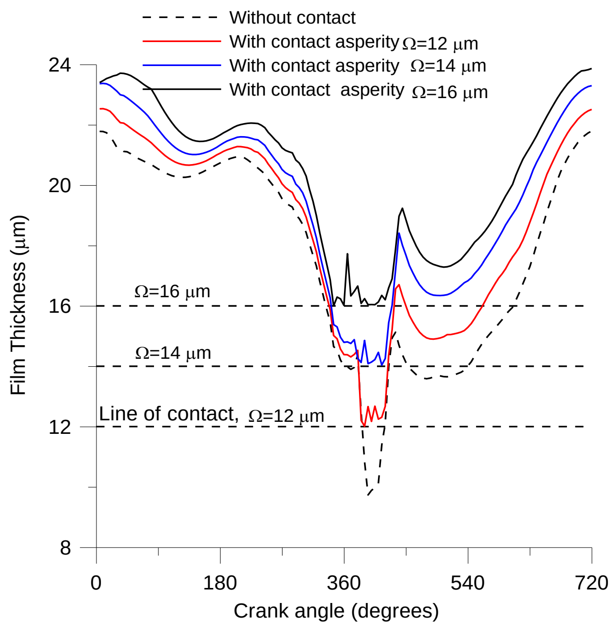

Fig. 10. Effect of the waviness surface of the skirt on the minimum film thickness for an engine speed of 1000 rpm.

The results show that the magnitude of the contact pressure is significantly higher than the hydrodynamic pressure, with a difference of about 2-3 MPa. The maximum values of the contact and hydrodynamic pressure, as well as the minimum film thickness, occur just after the top dead center at the power stroke. When the amplitude is the higher, $\Omega_3 = 16$ μm, the contact crank angle range widens further and begins even before the combustion gases ignite, as shown in Figure 11c.

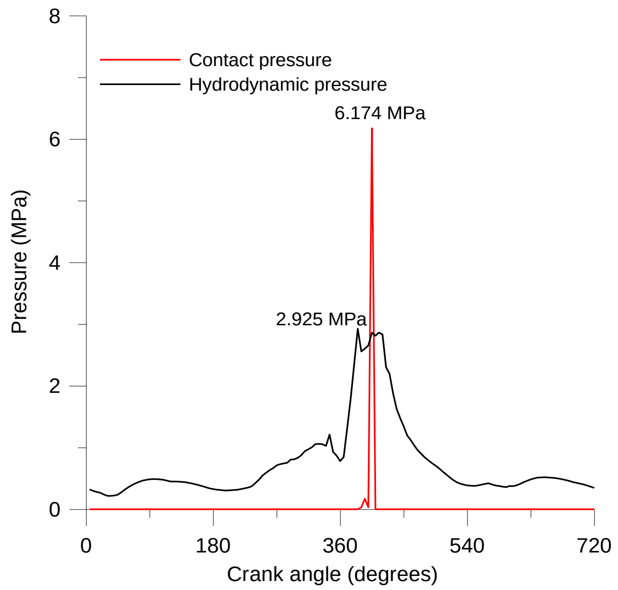

(a)

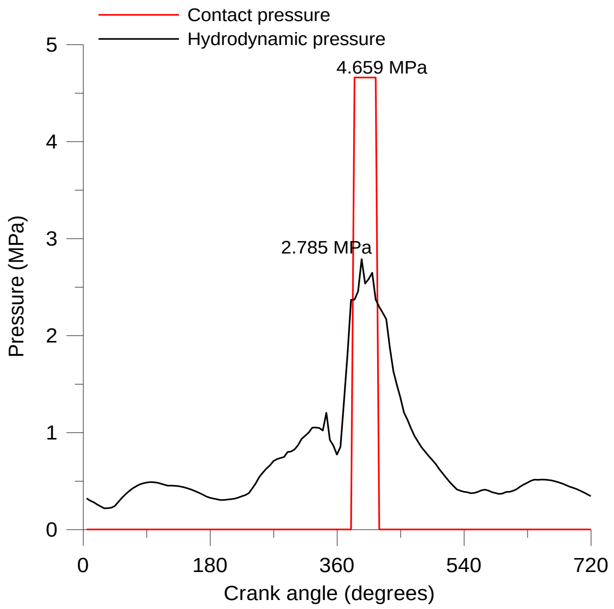

(b)

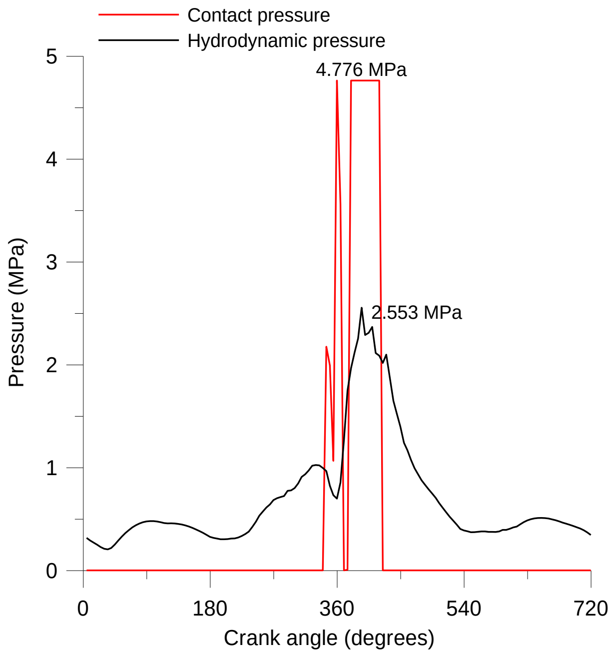

(c)

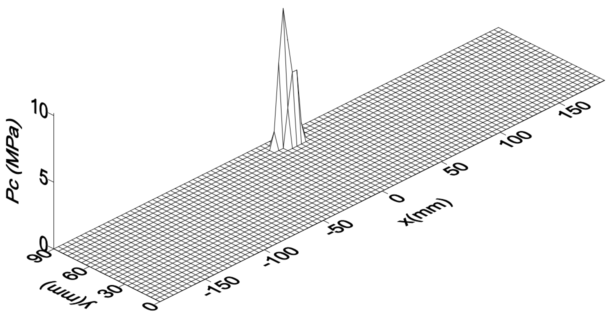

(d)

Fig. 11. Effect of the waviness surface of the skirt on the contact and hydrodynamic pressures (a) $\Omega_1 = 12\ \mu\text{m}$, (b) $\Omega_2 = 14\ \mu\text{m}$, (c) $\Omega_3 = 16\ \mu\text{m}$ and (d) distribution of the maximum contact pressure at a crank angle $\beta = 405°$ at V=1000 rpm.

When the amplitude of the asperity increases, the contact crank angle range expands from $[395°, 405°]$ to $[345°, 420]$. However, when the amplitude is smallest, the maximum contact pressure is higher, whereas for Ω_2 and Ω_3 it becomes nearly constant, with values of 4.659 MPa and 4.775 MPa, respectively. Figure 11d shows the distribution of the maximum contact pressure at a 405° crank angle, which takes place at the bottom of the skirt, for the smallest amplitude, $\Omega_1 = 12\ \mu\text{m}$. The obtained result is similar to that obtained by Sun et al. [18].

The corresponding eccentricities are obtained for each asperity amplitude and plotted in Figures 12a and 12b. The results show that as the waviness amplitude increases, the bottom eccentricity decreases and the top eccentricity increases, resulting in a reduced amplitude of the secondary movement.

Figure 12a shows that contact occurs at the bottom of the skirt toward the major thrust side during the power stroke, while the top of the piston moves toward the anti-thrust side. This configuration corresponds to mode 1, in accordance with the four possible contact modes of piston-cylinder described in [14]. The specific values of the secondary movement and the tribological characteristics are given in Table 2. The position $\overline{\Omega}_i$ of the contact line (on the y-axis of Figures 12a and 12b) is evaluated according to the relation $\overline{\Omega}_i = r - e_{imin}$, $i = 1{,}3$, where r is the radial clearance (taken as negative for the case of thrust side direction and positive for the case of anti-thrust side), e_i is the minimum or maximum eccentricity after contact deformation. The index i refers to the amplitude number.

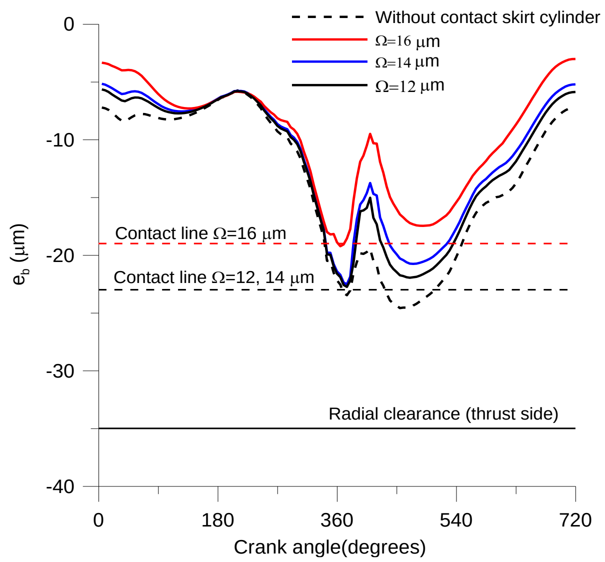

(a)

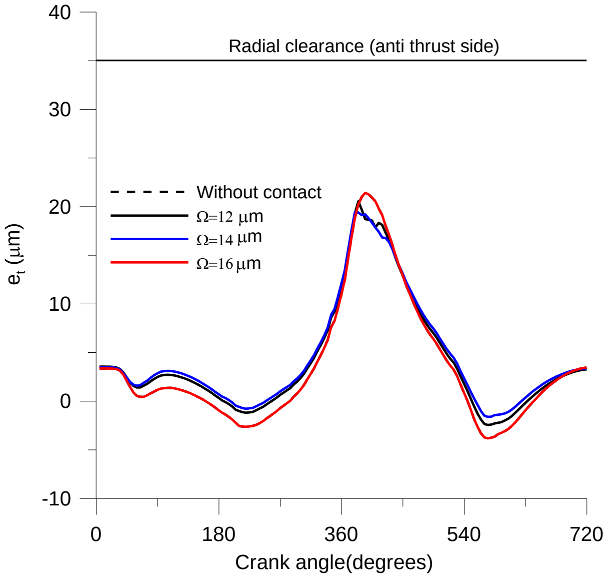

(b)

Fig. 12. Effect of the skirt surface waviness on (a) the bottom eccentricity and (b) the top eccentricity at V=1000 rpm.

Table 2. Specific values of the secondary movement and the tribological characteristics according to the skirt surface waviness, where $[e_{bmin}, e_{tmax}(e_{imin})]$= [minimum bottom eccentricity, maximum top eccentricity] and $[P_{cmax}, P_{hmax}]$= [maximum contact pressure, maximum hydrodynamic pressure].

Ω [μm]	e_{bmin}, [µm], β [°]	e_{tmax} [µm], β [°]	P_{cmax} [MPa], β [°]	P_{hmax}[MPa], β [°]
Without contact	-23.47, 375	21.39, 395	0	3.63, 395
$\Omega = 12$	−22.75, 375	20.51, 385	6.174, [395, 405]	2.925, 385
$\Omega = 14$	-22.53, 375	19.42 , 380	4.659, [385, 415]	2.785, 385
$\Omega = 16$	-19.23, 365	18.25, 380	4.776, [345, 420]	2.553, 385

4.4 Effect of the waviness on the thrust loads

The effect of waviness asperity contact on the carrying (thrust) loads, which result from asperity contact in the mixed lubrication zone and from hydrodynamic lubrication, is shown in Figure 13. The maximum values are highlighted for the different amplitudes on the curves of asperity contact load, hydrodynamic load, and total carrying load in Figures 13a–13c.

The hydrodynamic loads are much higher compared to the contact loads, whereas, conversely, the contact pressures are much higher than the hydrodynamic pressures, as shown in Figure 11.

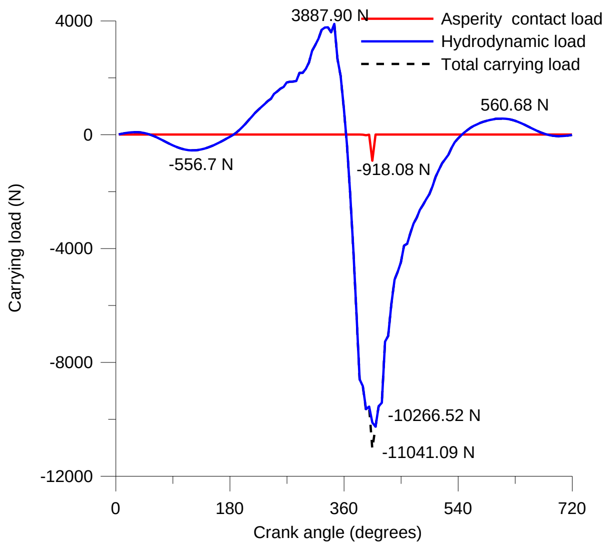

(a)

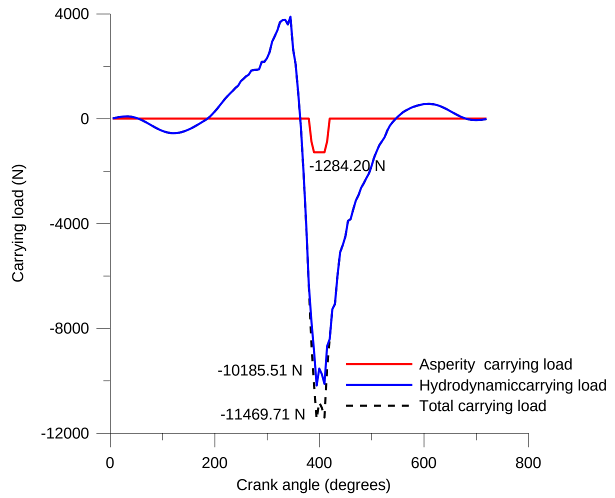

(b)

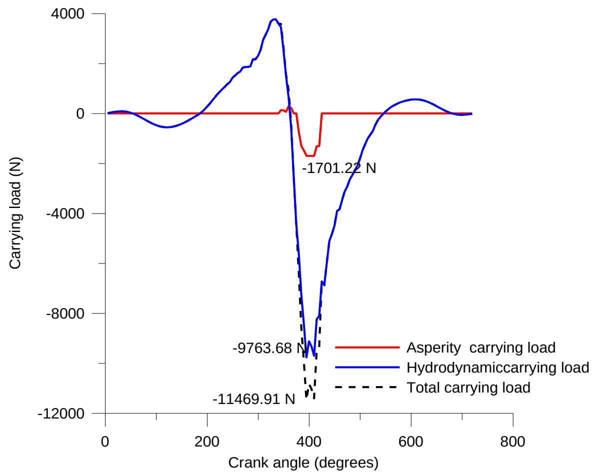

(c)

Fig. 13. Effect of the waviness surface of the skirt on the contact and hydrodynamic carrying loads (a) $\Omega_1 = 12$ µm, (b) $\Omega_2 = 14$ µm, and $\Omega_3 = 16$ µm at V=1000 rpm.

This result is explained by the fact that the contact surface is very small compared to the much larger lubricated surface Ω_h of the skirt. The results show that the hydrodynamic load reaches its maximum value of -10266.52 N just after the top dead center, at 395° during the power stroke, with a negative value toward the thrust side. This result is consistent with the piston configuration at 395°, as indicated by the curve of eccentricities in Figure 12, where the piston is displaced towards the anti-thrust side. This displacement causes the lubricating film to generate a carrying load acting in the opposite direction, toward the thrust side.

The results in Figure 13 also show that the hydrodynamic load reaches its maximum absolute values after bottom dead center or top dead center at each mid-stroke. This is due to the fact that, at these points, the hydrodynamic pressure is at its maximum value, as shown in Figures 11a-11c. This result is similar to that obtained by Zhu et al. [11,12]. The results further show that when the amplitude of the asperity increases, the hydrodynamic load decreases from -10266.52 N to -9763.68 N and the contact load increases from -918.08 N to -1701.22 N.

4.5 Effect of waviness on the sliding contact friction

Figure 14 shows the effect of the wavy asperities on the sliding contact friction according to the Bowden-Tabor model and the comparison with the hydrodynamic friction generated in the lubricant oil film.

The coefficient of contact friction μ_P is calculated according to relation (8) with the mean maximum value $\bar{\mu}_{\text{Pmax}} = \frac{2\Omega}{\lambda}$ obtained for $\bar{\delta}_{i\,max} = \Omega_i$, i=1,3, where the index i refers to the amplitude number. The experimental value of the coefficient of sliding friction of the piston-cylinder is obtained by the variable incidence tribometer presented in section 3. Three skirt pistons are used with surface waviness of approximate amplitudes Ω_1, Ω_2, and Ω_3. The corresponding values of the coefficients of sliding friction are 0.12, 0.22, and 0.30, respectively.

The designation of the four piston strokes is highlighted in Figure 14a to verify the consistency between the opposing directions of the friction load and the piston displacement. The contact friction occurs just after the TDC for the lower amplitudes of 12 μm and 14 μm and, it acts over a wide crank angle range before and after the TDC of the power stroke for the higher amplitude of 16 μm as shown in figure 14c. The location of the contact interval is consistent with that of the contact pressure presented in Figure 11c. The result is similar to that obtained by Liu et al. [21]. The results show mainly that the coefficient of the sliding friction is not constant but varies with the asperity amplitude, increasing from $\mu_P = 0.096$ to 0.128 as the amplitude increases from 12 to 16 μm**.** The results show that the sliding contact friction and the energy loss increase as the amplitude of the asperity increases.

The lowest values corresponding to the amplitude $\Omega = 12$ μm are -918.08 N and 0.054 J for the sliding friction and the energy loss, while the hydrodynamic load friction and the corresponding energy loss are not affected by the asperity amplitude. Therefore, reducing the energy loss due to sliding contact can be achieved by decreasing the asperity amplitude at a fixed engine speed. Thus, for a given engine speed in mixed lubrication, the reduction of contact energy loss is obtained in a similar manner by using section 4.1 to identify the minimum contact amplitude and section 4.5 to evaluate the energy loss due to sliding contact friction.

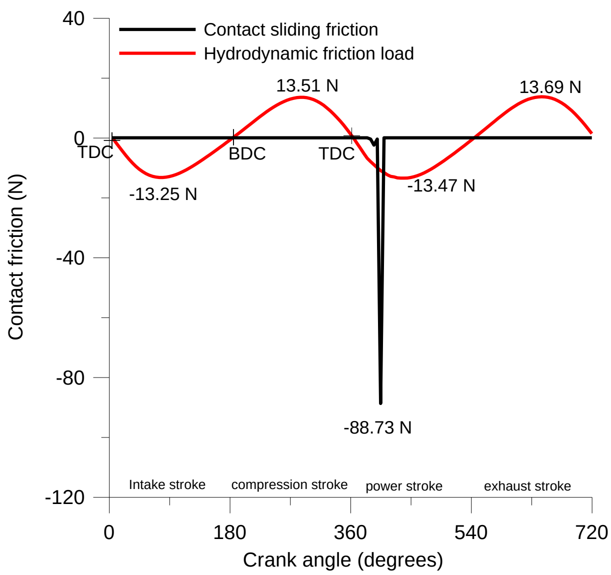

(a) $\mu_P = 0.096$

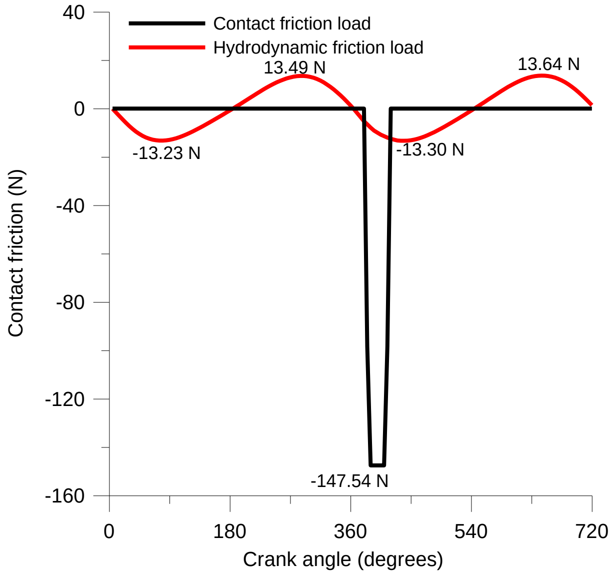

(b) $\mu_P = 0.112$

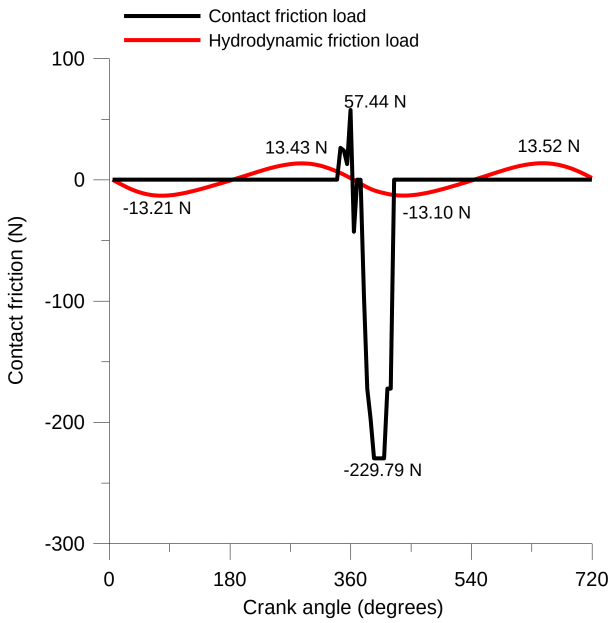

(c) $\mu_P = 0.128$

Fig. 14. Effect of the waviness surface of the skirt on the sliding contact and hydrodynamic friction with the corresponding contact range (a) $\Omega_1 = 12$ µm, [395, 405°] (b) $\Omega_2 = 14$ µm, [385,415°] and $\Omega_3 = 16$ µm, [345,425] at V=1000 rpm.

Table 3. Frictional energy loss (total lost enery E_f , energy loss by contact E_c and the hydrodynamic energy loss E_h) for fixed amplitude of asperities.

Ω (µm)	E_c (J)	E_h (J)	E_f (J)	E_c/E_f (%)
12	0.054	0.1588	0.212	25.47
14	0.555	0.1586	0.713	77.84
16	1.126	0.1586	1.284	87.69

5. CONCLUSION

This study is a part of a research effort on engine design aimed at reducing energy losses due to friction in the piston-cylinder system. A numerical model of a real piston-cylinder of a heavy truck in mixed lubrication was developed to determine the effect of lubrication performance and wavy asperity contact on the tribological characteristics, mainly on asperity sliding friction. The following results were:

- The mixed lubrication analysis shows the necessity of considering the elasticity of both the skirt and the cylinder to accurately solve the solid-to-solid asperity contact model, as well as the need to account for cavitation to ensure the consistency of the results.
- The waviness profile of the skirt surface has a significant effect on the tribological characteristics. The results show that all the tribological characteristics-contact pressure, sliding friction load, energy loss, and the coefficient of friction-increase with the asperity amplitude increases.
- Contact pressure and sliding contact friction act over a short interval with amplitudes higher than those of hydrodynamic friction. The contact interval extends as the asperity amplitude increases. When the amplitude increases from 12 to 16 µm, the coefficient of sliding friction increases from $\mu_P = 0.096$ to 0.128 and the contact energy loss over one engine cycle increases from 0.054 J to 1.126 J, representing 25% to 78% of the total energy loss, respectively.
- The hydrodynamic friction load and the corresponding energy loss are not affected by the asperity amplitude. Therefore, reducing the energy loss due to sliding contact friction in mixed lubrication can be achieved by minimizing the amplitude of the asperity contact at a fixed engine speed.

Acknowledgement

The authors would like to thank the Direction Générale de la Recherche Scientifique et du Développement Technologique (DGRSDT), Algiers, Algeria, for its contribution to this article.

REFERENCES

[1] D. E. Richardson, "Review of power cylinder friction for diesel engines," *Journal of Engineering for Gas Turbines and Power*, vol. 122, no. 4, pp. 506–519, Apr. 2000, doi: 10.1115/1.1290592.

[2] V. W. Wong and S. C. Tung, "Overview of automotive engine friction and reduction trends–Effects of surface, material, and lubricant-additive technologies," *Friction*, vol. 4, no. 1, pp. 1–28, Mar. 2016, doi: 10.1007/s40544-016-0107-9.

[3] P. Nagar and S. Miers, "Friction between Piston and Cylinder of an IC Engine: a Review," *SAE Technical Papers on CD-ROM/SAE Technical Paper Series*, vol. 1, Apr. 2011, doi: 10.4271/2011-01-1405.

[4] K. Holmberg, P. Andersson, and A. Erdemir, "Global energy consumption due to friction in passenger cars," *Tribology International*, vol. 47, pp. 221–234, Dec. 2011, doi: 10.1016/j.triboint.2011.11.022.

[5] C. Delprete, C. Gastaldi, and L. Giorio, "A minimal input engine friction model for power loss prediction," *Lubricants*, vol. 10, no. 5, p. 94, May 2022, doi: 10.3390/lubricants10050094.

[6] A. Sydbom, A. Blomberg, S. Parnia, N. Stenfors, T. Sandström, and S. Dahlén, "Health effects of diesel exhaust emissions," *European Respiratory Journal*, vol. 17, no. 4, pp. 733–746, Apr. 2001, doi: 10.1183/09031936.01.17407330.

[7] A. Fayyazbakhsh *et al.*, "Engine emissions with air pollutants and greenhouse gases and their control technologies," *Journal of Cleaner Production*, vol. 376, p. 134260, Sep. 2022, doi: 10.1016/j.jclepro.2022.134260.

[8] İ. A. Reşitoğlu, K. Altinişik, and A. Keskin, "The pollutant emissions from diesel-engine vehicles and exhaust aftertreatment systems," *Clean Technologies and Environmental Policy*, vol. 17, no. 1, pp. 15–27, Jun. 2014, doi: 10.1007/s10098-014-0793-9.

[9] H. A. Spikes and A. V. Olver, "Mixed lubrication—Experiment and theory," in *Tribology series*, 2002, pp. 95–113, doi: 10.1016/S0167-8922(02)80011-6.

[10] H. A. Spikes, "Mixed lubrication — an overview," *Lubrication Science*, vol. 9, no. 3, pp. 221–253, May 1997, doi: 10.1002/ls.3010090302.

[11] D. Zhu, H. S. Cheng, T. Arai, and K. Hamai, "A Numerical Analysis for Piston Skirts in Mixed Lubrication—Part I: Basic Modeling," *Journal of Tribology*, vol. 114, no. 3, pp. 553–562, Jul. 1992, doi: 10.1115/1.2920917.

[12] D. Zhu, Y.-Z. Hu, H. S. Cheng, T. Arai, and K. Hamai, "A Numerical Analysis for piston skirts in mixed lubrication: Part II—Deformation considerations," *Journal of Tribology*, vol. 115, no. 1, pp. 125–133, Jan. 1993, doi: 10.1115/1.2920965.

[13] N. Patir and H. S. Cheng, "An average flow model for determining effects of Three-Dimensional roughness on partial hydrodynamic lubrication," *Journal of Lubrication Technology*, vol. 100, no. 1, pp. 12–17, Jan. 1978, doi: 10.1115/1.3453103.

[14] D. F. Li, S. M. Rohde, and H. A. Ezzat, "An automotive Piston lubrication model," *A S L E Transactions*, vol. 26, no. 2, pp. 151–160, Jan. 1983, doi: 10.1080/05698198308981489.

[15] K. L. Johnson, Contact Mechanics. Cambridge University Press, 1985, doi: 10.1017/cbo9781139171731.

[16] Z. Jin, Z. Z. Yu, and L. S. Yang, "Prediction of Nonlinear Contact Force of Piston Skirt and Cylinder Liner under the Function of Clap Force," *Applied Mechanics and Materials*, vol. 226–228, pp. 831–834, Nov. 2012, doi: 10.4028/www.scientific.net/AMM.226-228.831.

[17] L. Ning, X. Meng, and Y. Xie, "Effects of lubricant shear thinning on the mixed lubrication of piston skirt-liner system," *Proceedings of the Institution of Mechanical Engineers Part C Journal of Mechanical Engineering Science*, vol. 227, no. 7, pp. 1585–1598, Sep. 2012, doi: 10.1177/0954406212460610.

[18] J. Sun *et al.*, "Research on the lubrication performance of engine piston skirt–cylinder liner frictional pair considering lubricating oil transport," *International Journal of Engine Research*, vol. 21, no. 4, pp. 713–722, Jun. 2018, doi: 10.1177/1468087418778658.

[19] J. A. Greenwood and J. H. Tripp, "The contact of two nominally flat rough surfaces," *Proceedings of the Institution of Mechanical Engineers*, vol. 185, no. 1, pp. 625–633, Jun. 1970, doi: 10.1243/PIME_PROC_1970_185_069_02.

[20] Z. Meng, L. Zhang, T. Tian, "Study of Break-In Process and its effects on Piston Skirt Lubrication in Internal Combustion Engines," *Lubricants*, vol. 7, no. 11, pp. 1-18, Nov. 2019, doi: 10.3390/lubricants7110098.

[21] N. Liu, C. Wang, Q. Xia, Y. Gao, P. Liu, "Simulation on the effect of cylinder liner and piston ring surface roughness on friction performance," *Mechanics & Industry*, vol. 23, no. 8, pp. 1-13, Jun. 2022, doi: 10.1051/meca/2022007.

[22] B. Zhao, S. Wang, P. Xiao, L. Xu, X. Hu, X. Si and Y. Liu, "The Tribo-Dynamics Performance of the Lubricated Piston Skirt–Cylinder System Considering the Cylinder Liner Vibration," *Lubricants*, vol. 10, no. 11, pp. 1-21, Nov. 2022, doi: 10.3390/lubricants10110319.

[23] F. P. Bowden and D. Tabor, *The friction and lubrication of solids*. 2001. doi: 10.1093/oso/9780198507772.001.0001.

[24] F. Mc Clure, "Numerical Modeling of Piston Secondary Motion and Skirt Lubrication in Internal Combustion Engines," Ph.D. Thesis, Massachusetts Institute of Technology, Cambridge, MA, USA, 2007.

[25] E. M. Feghoul, A. Belalia, H. Aboshighiba, and M. Tahar Abbes, "*Cavitation modeling effect on tribological performances in piston skirt lubrication*," Jurnal Tribologi, vol. 42, pp. 198-215, Aug. 2024.

[26] H. Hertz, "Ueber die Berührung fester elastischer Körper.," *Journal Für Die Reine Und Angewandte Mathematik (Crelles Journal)*, vol. 1882, no. 92, pp. 156–171, Jan. 1882, doi: 10.1515/crll.1882.92.156.

[27] N. Patir and H. S. Cheng, "Application of average flow model to lubrication between rough sliding surfaces," *Journal of Lubrication Technology*, vol. 101, no. 2, pp. 220–229, Apr. 1979, doi: 10.1115/1.3453329.

[28] A. Akchurin, R. Bosman, P.M Lugt, and M. V. Drogen, "On a Model for the Prediction of the Friction Coefficient in Mixed Lubrication Based on a Load-Sharing Concept with Measured Surface Roughness." *Tribology Letters*, vol. 59 no. 1, pp. 1-11, July. 2015, doi: 10.1007/s11249-015-0536-z.

[29] K..G. Murty, "Note on a Bard-type scheme for solving the complementarity problem," Opsearch, vol. 11, pp. 123-130, 1974.

[30] D. Guines, "La Lubrification des Liaisons Compliantes: Modélisation et Algorithmes," Ph.D. dissertation, Dept. Mech. Eng., Poitiers Univ., Poitiers, 1994.

[31] H. G. Elrod, "A cavitation algorithm," *Journal of Lubrication Technology*, vol. 103, no. 3, pp. 350–354, Jul. 1981, doi: 10.1115/1.3251669.

[32] T. Kelemenová *et al.*, "Specific problems in measurement of coefficient of friction using variable incidence tribometer," *Symmetry*, vol. 12, no. 8, p. 1235, Jul. 2020, doi: 10.3390/sym12081235.

[33] G. W. Stachowiak and A. W. Batchelor, Experimental Methods in Tribology, 1st Ed., vol. 44, Elsevier Science, 2004.